PHYSICAL REVIEW B **87**, 220101(R) (2013)

Uniaxial strain-induced ferroelectric phase with a giant axial ratio in a (110) $BiFeO_3$ thin film

Huajun Liu,[1] Ping Yang,[2] Zhen Fan,[1] Amit Kumar,[3] Kui Yao,[4] Khuong Phuong Ong,[5] Kaiyang Zeng,[3] and John Wang[1,*]

[1]*Department of Materials Science and Engineering, National University of Singapore, Singapore*

[2]*Singapore Synchrotron Light Source (SSLS), National University of Singapore, Singapore*

[3]*Department of Mechanical Engineering, National University of Singapore, Singapore*

[4]*Institute of Materials Research and Engineering, A*STAR (Agency for Science, Technology and Research), Singapore*

[5]*Institute of High Performance Computing, A*STAR (Agency for Science, Technology and Research), Singapore*

(Received 28 December 2012; revised manuscript received 15 May 2013; published 6 June 2013)

Strain engineering, which employs biaxial misfit strain to deform the crystal structure, is a powerful tool to tune the physical behavior of epitaxial thin films. Here we show that a 10-nm-thick $BiFeO_3$ film is uniaxially strained by (110)-oriented $LaAlO_3$ substrate, which exhibits a monoclinic lattice with a giant $c/a \sim 1.24$ and a unique stripe ferroelectric domain configuration, as revealed by high resolution synchrotron x-ray diffraction and piezoelectric force microscopy. A strain-phase diagram for $BiFeO_3$ under uniaxial strain condition is predicted by first-principles calculations, suggesting that monoclinic Pm phase with a large polarization of $\sim$130 $\mu C/cm^2$ is the lowest-in-energy phase when strained by (110)-oriented $LaAlO_3$ substrate. Our results provide a potential route to tune physical behavior of epitaxial ferroelectric thin films by uniaxial strain in (110) orientation, instead of widely investigated biaxial strain in (001) orientation.

DOI: 10.1103/PhysRevB.87.220101 PACS number(s): 77.80.−e, 77.55.−g, 75.85.+t

I. INTRODUCTION

In complex transition-metal oxides, the competition and cooperation of charge, spin, and orbital degrees of freedom, leads to the extreme sensitivity of physical properties to structure distortions and strain states of epitaxial thin films.[1] Substrate misfit strain is thus often employed to tune the crystal structure and therefore the physical behavior of epitaxial thin films, which is known as strain engineering.[2] It has been shown that epitaxial strain can double the superconducting transition temperature of $La_{2-x}Sr_xCuO_4$,[3,4] greatly enhancing ferroelectric polarization of $BaTiO_3$ (Ref. 5) and creating a multiferroic $EuTiO_3$ thin film.[6]

Most of the previous studies of strain engineering, however, focused only on the perovskite films with (001) pseudocubic orientation, where the biaxial strain is generated as a result of the isotropic nature of the in-plane $[100]_{pc}$ and $[010]_{pc}$ directions [Fig. 1(a)]. The strains on other crystallographic orientations are fundamentally different from (001) orientation, which may produce new crystal phases and novel functionalities that are not available in (001) orientation. Take (110) orientation for example; the strain is anisotropic due to the different atomic arrangement and lattice dimension along the in-plane $[001]_{pc}$ and $[\bar{1}10]_{pc}$ directions [Fig. 1(b)]. This leads to a unique and interesting effect of strain on the physical behavior of (110)-oriented films. For instance, charge and orbital order cannot be realized in (001) and (111) films but is stabilized in (110)-oriented $Nd_{1-x}Sr_xMnO_3$ film.[7] Another example is controlling in-plane magnetic anisotropy by (110)-oriented substrates in epitaxial perovskite manganite films.[8] In addition, anisotropic Josephson junctions can be achieved in (110)-oriented superconductor thin films.[9]

$BiFeO_3$ (BFO) is a multiferroic material, showing a coupling between antiferromagnetism and ferroelectric order at room temperature.[10] The effect of biaxial strain on the crystal phase and physical behavior of (001)-orientated BFO epitaxial thin films has been the focus of recent theoretical and experimental studies.[11–14] Although tremendous work has been done in strain engineering of BFO in (001) orientation, very few reports investigated BFO film in other orientations[15,16] and no systematic strain effect has been experimentally studied in (110) orientation. By using high resolution synchrotron x-ray diffraction (XRD), we show that substrate misfit strain in (110) orientation is uniaxial, instead of biaxial nature in (001) orientation. More interestingly, a large compressive uniaxial strain of $\sim$4.5% from (110) $LaAlO_3$ (LAO) substrate can be employed to induce a BFO phase with a giant axial ratio $c/a \sim 1.24$ and a large twin angle of $\sim 26^\circ$, which is highly distorted compared to bulk structure. The ferroelectric nature of this BFO phase and strip domain structures are revealed by intensity modulation peaks in reciprocal space mappings (RSMs) and phase images from piezoelectric force microscopy (PFM). Our first-principles calculations, considering the uniaxial strain condition, show that the monoclinic space group Pm is the lowest-energy phase for BFO film under a compressive strain from -6% to -2.5%, which agrees well with the monoclinic BFO lattice determined experimentally. The promising physical behavior of this new BFO phase will also be discussed.

II. METHODOLOGY

Epitaxial BFO film was deposited directly on LAO substrate in (110) orientation by rf sputtering at 680 °C with sputtering power of 120 W and Ar/O_2 ratio of 14/5. The film thickness is $\sim$10 nm, which is determined from x-ray reflection. The crystal structure was investigated using high resolution synchrotron x-ray diffractometry at the XDD (x-ray development and demonstration) beam line of Singapore Synchrotron Light Source (SSLS) and the BL14B1 beam line of Shanghai Synchrotron Radiation Facility (SSRF). Ferroelectric domain structure was studied by a commercial scanning probe microscope (MFP-3D, Asylum Research, USA) in vector PFM mode. First-principles calculations were performed using the Vienna *ab initio* simulation package (VASP)[17] within the generalized gradient approximation in

 ©2013 American Physical Society

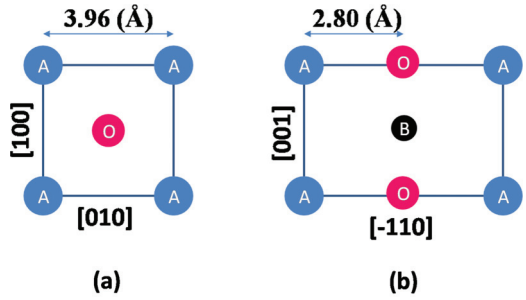

FIG. 1. (Color online) Schematic atomic structure model for epitaxial growth of perovskite ABO_3 structure in (001) (a) and (110) (b) orientations. The lattice dimension of bulk BFO is shown.

the form proposed by Perdew, Burke, and Ernzerhof.[18] We used the projected augmented wave method with a plane-wave cutoff of 500 eV and a $3 \times 3 \times 3$ k-point mesh in the whole Brillouin zone.[19] The Bi ($5d^{10}6s^26p^3$), Fe ($3p^63d^64s^2$), and O ($2s^22p^4$) are chosen as valence states. The structures are fully relaxed till the Hellmann-Feynman forces were <2 meV/Å. The electronic polarization was calculated using the Berry phase method.[20,21] The total energies of different phases are benchmarked with the rhombohedral R-3c with lattice vector $a = b = c = 4.0$ Å.

III. RESULTS AND DISCUSSION

Figure 2(a) shows an x-ray diffraction θ-2θ scan of BFO film on LAO (110) substrate, with only diffraction peaks from pseudocubic (110) and (220) observed. From these diffraction angles, the d spacing of BFO (110) is determined to be ~2.985 Å, larger than that of bulk BFO (~2.80 Å). This indicates an elongation of out-of-plane (OP) lattice dimension, which is a result of the in-plane (IP) compression from LAO substrate. However, the amount of elongation is quite small here considering the large mismatch between LAO and BFO, which stretches the OP lattice parameter from ~4.0 to 4.6 Å in the film of (001) orientation.[14] To further understand the crystal structure, RSMs were measured by coplanar diffraction geometry [Figs. 2(b)–2(d)]. The axes for the RSMs are arranged in such a way that a direction orients along $[\bar{1}10]_{pc}$, b along $[001]_{pc}$, and c along $[110]_{pc}$ [Fig. 2(e)]. The reciprocal lattice units are based on the lattice parameters of LAO substrate, with $2\pi/2.68$ Å^{-1} along H and L, and $2\pi/3.79$ Å^{-1} along K. Both $(001)_{KL}$ and $(0\bar{1}2)_{KL}$ RSMs [Figs. 2(b) and 2(c)] show a single diffraction peak from BFO film with the same K value as the substrate. This indicates that BFO film is fully coherent along the $[001]_{pc}$ direction. Interestingly, $(\bar{1}02)_{HL}$ RSM shows a vertical splitting of BFO diffraction peaks located at a H position different from the substrate, indicating that a twin structure

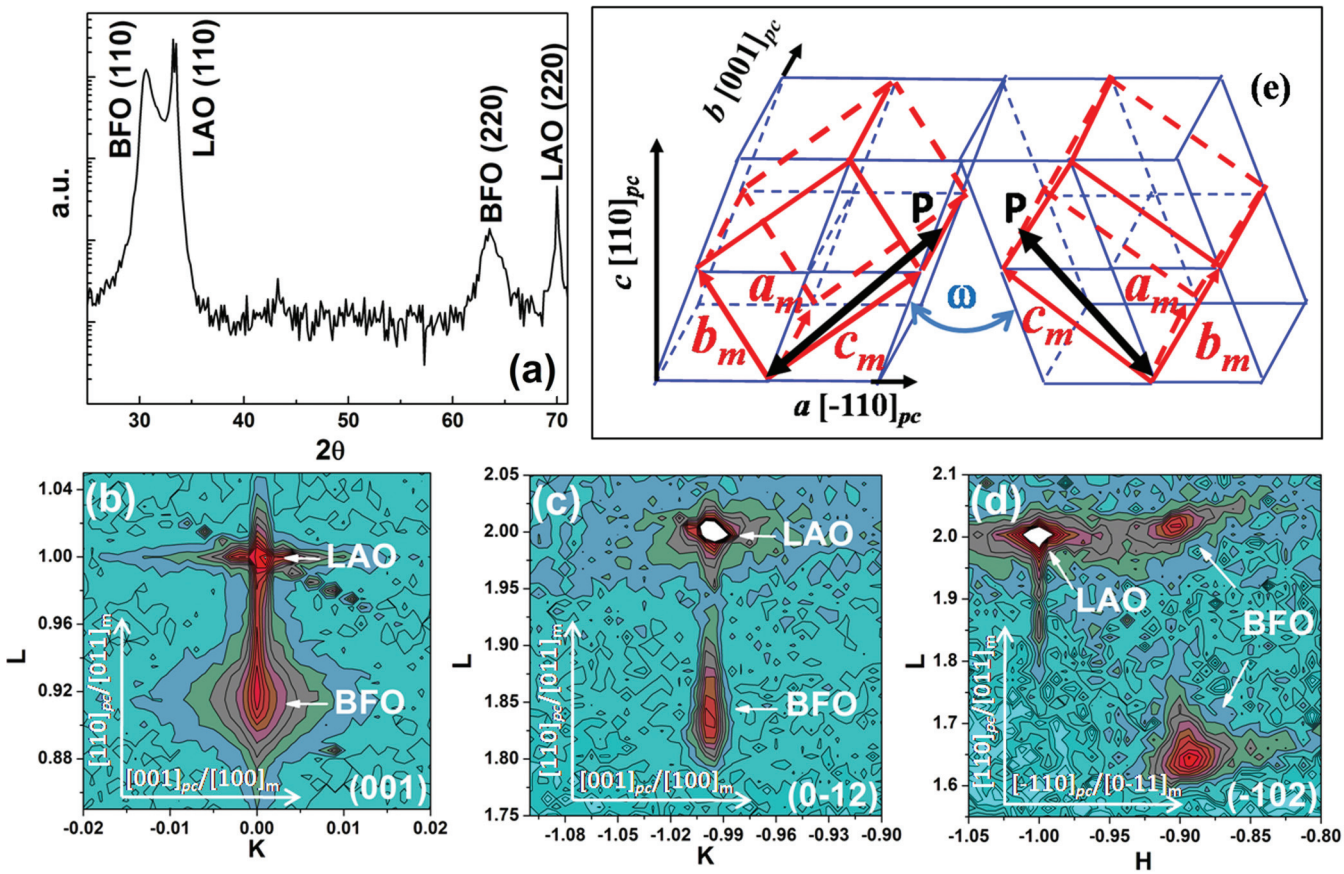

FIG. 2. (Color online) (a) X-ray diffraction θ-2θ scan of BFO film grown on LAO (110) substrate. Reciprocal space mappings around $(001)_{KL}$ (b), $(0\bar{1}2)_{KL}$ (c), and $(\bar{1}02)_{HL}$ (d) are indexed in the lattice with a, b, and c along $[\bar{1}10]_{pc}$, $[001]_{pc}$, and $[110]_{pc}$, respectively [as labeled in (e)]. The unit cell with thick lines (a_m, b_m, and c_m) shows a schematic structure model of BFO (e).

is formed along the H direction. Surprisingly, this vertical splitting distance along L is huge, which corresponds to the angle between two domains ω as large as $\sim 26^\circ$ [Fig. 2(e)]. The lattice dimension of BFO film along the $[\bar{1}10]_{pc}$ direction is ~ 3.003 Å, which is larger than the lattice dimension of bulk BFO (~ 2.80 Å), as shown in Fig. 1(b). This suggests that the strain along the $[\bar{1}10]_{pc}$ direction is relaxed even in the film with a thickness of ~ 10 nm, which clearly shows that strain in (110)-oriented film is uniaxial along the $[001]_{pc}$ direction. A previous study in epitaxial manganite (110) films also shows that the lattice dimension along the $[001]_{pc}$ direction is locked by the substrate, while the lattice dimensions along the $[110]_{pc}$ and $[\bar{1}10]_{pc}$ directions vary drastically as the temperature changes.[22] It should be noted that there is one oxygen atom along the $[\bar{1}10]_{pc}$ direction but no oxygen atom along the $[001]_{pc}$ direction [Fig. 1(b)]. This indicates that oxygen octahedral rotation, which has an effect along the $[\bar{1}10]_{pc}$ direction but not along the $[001]_{pc}$ direction, may be responsible for the uniaxial strain state in the (110) orientation.

The observation of a $(-1/2,0,3/2)$ diffraction peak (not shown) suggests that the BFO unit cell should be reselected along the diagonal directions in the ac plane in order to represent the real symmetry of the lattice. The lattice parameters are calculated as $a_m = 3.790$ Å, $b_m = 3.731$ Å, $c_m = 4.684$ Å, $\alpha = \gamma = 90^\circ$, and $\beta = 90.37^\circ$. This new lattice is schematically drawn by the thick lines in Fig. 2(e), with a_m, b_m, and c_m along the $[001]_{pc}$, $[100]_{pc}$, and $[010]_{pc}$ directions, respectively. Therefore, the 10-nm-thick BFO film on LAO (110) substrate has a monoclinic lattice with a giant c/a ratio of ~ 1.24, which is slightly distorted by 0.37° from an orthorhombic lattice.

To characterize the ferroelectric nature of ultrathin film, direct measurement by polarization-electric field hysteresis loops using a Sawyer-Tower circuit is difficult due to high leakage current and large coercive field.[13,23] Alternatively, the modulation peaks in x-ray diffraction can be employed to study the ferroelectric domain structures and the polarization direction, as reported in previous studies.[24,25] Due to the different atomic shift in each ferroelectric domain, the x-ray diffraction structure factor has a contrast along the direction perpendicular to stripe domain walls, leading to the intensity modulation. If the reciprocal space vector $\boldsymbol{q}_{(HKL)}$ is perpendicular to the polar shift direction, no modulation peak would be detected. Whereas if $\boldsymbol{q}_{(HKL)}$ has a component parallel to the polar shift direction, modulation peaks will occur. Therefore, the Bragg peaks (HKL), around which the modulation peaks appear, give the information about the polar shift direction, i.e., the polarization direction.

Figure 3 shows the $(001)_{HL}$, $(010)_{HK}$, and $(100)_{HK}$ RSMs. The in-plane RSMs (100) and (010) were measured by grazing incident x-ray diffraction using a six-circle diffractometer at SSRF. In (001) RSM [Fig. 3(a)], in addition to the strong

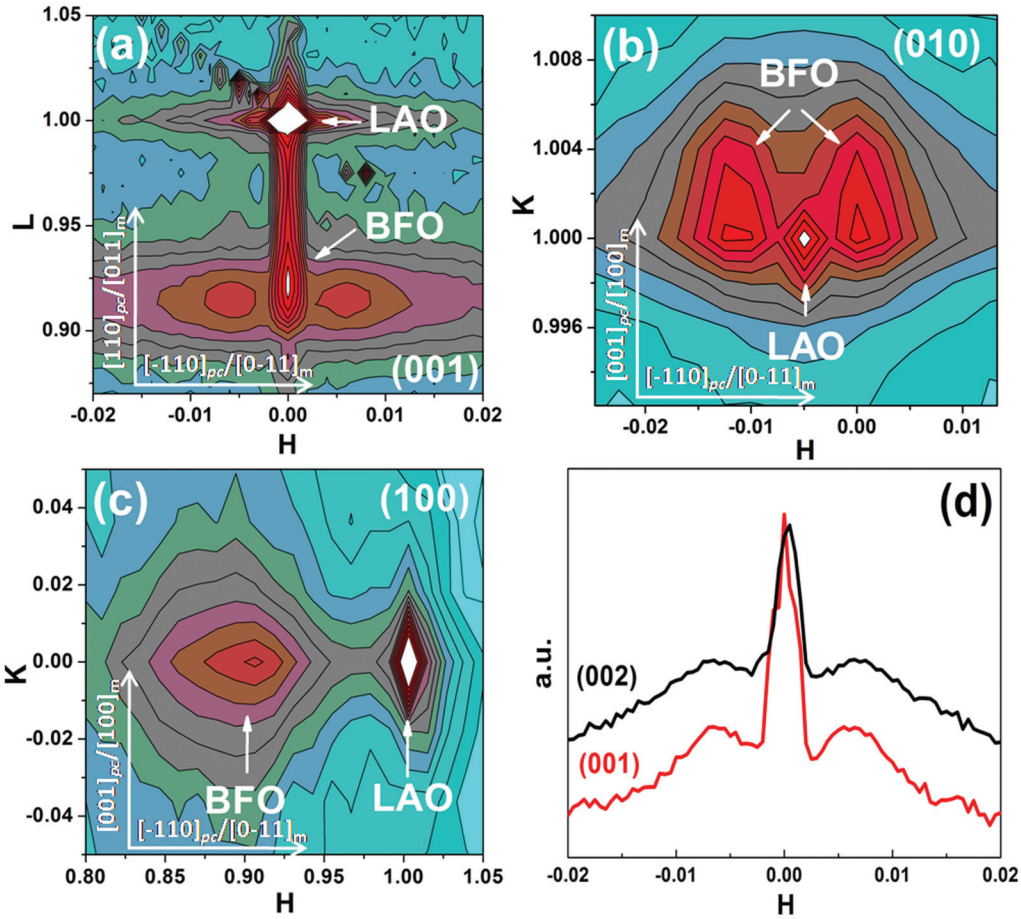

FIG. 3. (Color online) Reciprocal space mappings around $(001)_{HL}$ (a), $(010)_{HK}$ (b), and $(100)_{HK}$ (c) for BFO film grown on LAO substrate. (d) H scan of BFO modulation peaks around (001) and (002).

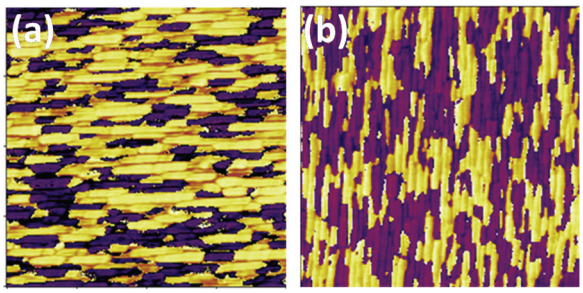

FIG. 4. (Color online) OP-PFM (a) and IP-PFM (b) phase image of BFO film grown on LAO substrate (scan area 2 μm $\times$ 2 μm). The IP-PFM images are taken along the H ($[\bar{1}10]_{pc}/[0\bar{1}1]_m$) direction.

sharp BFO diffraction peak at $H = 0$, two satellite peaks appear symmetrically around the BFO peak, with H values at -0.0065 and $+0.0065$, respectively. The two satellite peaks around the (002) peak also show the same H values [Fig. 3(d)]. Moreover, all other satellite peaks observed in this sample share the same separation distance ΔH between modulation peaks (not shown). This suggests that these satellite peaks are from the in-plane modulation, instead of the twinning structure.[26,27] Due to the in-plane uniaxial strain for (110) substrate, the modulation is only observed along the H direction, which is perpendicular to the ferroelectric domain wall direction. In (010) RSM [Fig. 3(b)], the main diffraction peak overlaps with the substrate peak, confirming the coherent growth along the K direction. The modulation peaks are also clearly observed with the same ΔH as in (00L) RSMs. For (100) RSM [Fig. 3(c)], a single BFO diffraction peak was observed with the same K value as the substrate, but a different H value. This is consistent with ($\bar{1}02$) RSM in Fig. 2(d). The FWHM (full width at half maximum) of this (100) peak is too broad to resolve the satellite peaks if they exist. Therefore, the existence or extinction of (100) modulation peaks cannot be determined. What can be confirmed for the RSM data is that BFO film shows modulation for the (00L) and (0K0) peaks, suggesting the polarization direction has projections along the $[001]_{pc}$ and $[110]_{pc}$ directions.

To clarify the polarization information along the $[\bar{1}10]_{pc}$ direction and verify the results from modulation peaks in RSMs, PFM is employed to study the polarization direction of BFO film. Figure 4(a) shows the OP-PFM phase image of BFO film, which clearly indicates a stripe ferroelectric domain structure with 180° phase contrast in the OP direction. This agrees with the observation of modulation peaks in (00L) diffraction peaks. The IP-PFM phase image along the H ($[\bar{1}10]_{pc}/[0\bar{1}1]_m$) direction is shown in Fig. 4(b), which also exhibits a stripe ferroelectric domain structure with 180° phase contrast. This means that the modulation peak should appear along the H direction. However, due to the board main Bragg peak, the modulation peaks cannot be seen in Fig. 3(c). The polarization of BFO film thus has out-of-plane projection along the L ($[110]_{pc}/[011]_m$) direction and in-plane projection slightly tilted away from the H ($[\bar{1}10]_{pc}/[0\bar{1}1]_m$) direction towards the K ($[001]_{pc}/[100]_m$) direction. Based on the monoclinic distortion of BFO lattice, the polarization direction should be slightly tilted away from the c_m axis within the $a_m c_m$ plane, because the monoclinic angle is very close to 90° and the c/a ratio has a giant value of ~1.24. This polarization direction is shown in Fig. 2(e), which is consistent with both RSMs modulation results and PFM data.

To understand this uniaxial strain-induced new BFO phase in the (110) orientation, we performed first-principles calculations. In order to mimic a perfect epitaxy on a (110) plane of LAO substrate following the description by our experiment, the lattice vectors are given by $\boldsymbol{a}_1 = 2a(0,1+\delta_1,0)$, $\boldsymbol{a}_2 = a(-1+\delta_2,\delta_2,1+\delta_3)$, and $\boldsymbol{a}_3 = a(1+\delta_2,\delta_2,1+\delta_3)$ in the new Cartesian (x,y,z) with x, y, and z along the $[001]_{pc}$, $[100]_{pc}$, and $[010]_{pc}$ directions, respectively. Here a is the lattice constant of the substrate. The $\boldsymbol{a}_1$, $\boldsymbol{a}_2$, and $\boldsymbol{a}_3$ lattice vectors are along the $[100]_{pc}$, $[0\bar{1}1]_{pc}$, and $[011]_{pc}$ directions, respectively. The uniaxial strain is assumed along the $[001]_{pc}$ direction as suggested by our experiment. A G-type antiferromagnetic order, constructed by $\boldsymbol{a}_1$, $\boldsymbol{a}_2$, and $\boldsymbol{a}_3$ accommodating a 20-atom unit cell, is imposed in our calculations. The misfit strain η_{mis} is defined as $\eta_{\text{mis}} = (a - a_0)/a_0$, with $a_0 = 3.96$ Å for bulk BFO. In order to compare with a previous report,[28] the *Pnma* phase is also calculated with biaxial strain applied along the $[001]_{pc}$ and $[\bar{1}10]_{pc}$ directions. The lattice vectors are given by $\boldsymbol{a}_1 = a(\sqrt{2},0,0)$, $\boldsymbol{a}_2 = a(0,2,0)$, and $\boldsymbol{a}_3 = a(0,0,\sqrt{2}+\delta_4)$ in the Cartesian (x',y',z') with x', y', and z' along the $[\bar{1}10]_{pc}$, $[001]_{pc}$, and $[110]_{pc}$ directions, respectively.

Depending on the values of δ_1, δ_2, and δ_3, four different phases has been obtained—monoclinic Pm, Cc, orthorhombic $Pmm2$, and tetragonal $P4mm$. A previous report on epitaxial ($\bar{1}10$) BFO thin film shows that the *Pnma* phase, which is centrosymmetric and paraelectric, is the most stable phase in the misfit strain range of $\sim -8\%$ to -1.6%.[28] However, it should be noted that the biaxial strain state is assumed in this calculation, which is inconsistent with the uniaxial strain state observed in our experiment. To clarify this issue, we built the *Pnma* phase model based on the biaxial constraint as described above. Different from that report, we found that the *Pnma* phase is not a stable phase in the misfit compressive strain range on epitaxial (110) BFO thin film [Fig. 5(a)]. Instead, monoclinic phases Pm and Cc are the most stable phases in the compressive misfit strain range from -6% to 0%. The monoclinic Cc phase is observed in the misfit strain from -2.5% to 0%, which agrees with the previous experimental results of the M_B phase for BFO film grown on STO (110) substrate at the misfit strain of $\sim -1.5\%$.[15] In the misfit strain from -6% to -2.5%, the monoclinic Pm phase is observed. This Pm phase possesses polarization along the $[u0v]_{pc}$ direction within one of the pseudocubic face planes, which is in good agreement with the polarization direction observed in our film. We notice that the energy differences between Pm, $Pmm2$, and $P4mm$ tend to be very small when the compressive misfit strain increases above 6%. This explains why the lattice parameters of our film are only slightly distorted from the orthorhombic lattice or tetragonal lattice. Figure 5(b) shows the calculated ferroelectric polarization as a function of misfit strain. For the Cc phase, the polarization is close to the $[111]_{pc}$ direction, leading to the polarization projection along all a, b, and c axes. For the Pm phase, as the compressive strain increases, the polarization along the c axis, P_c, tends to increase and approach ~120 μC/cm^2 and the polarization along the a axis, P_a, tends to decrease and

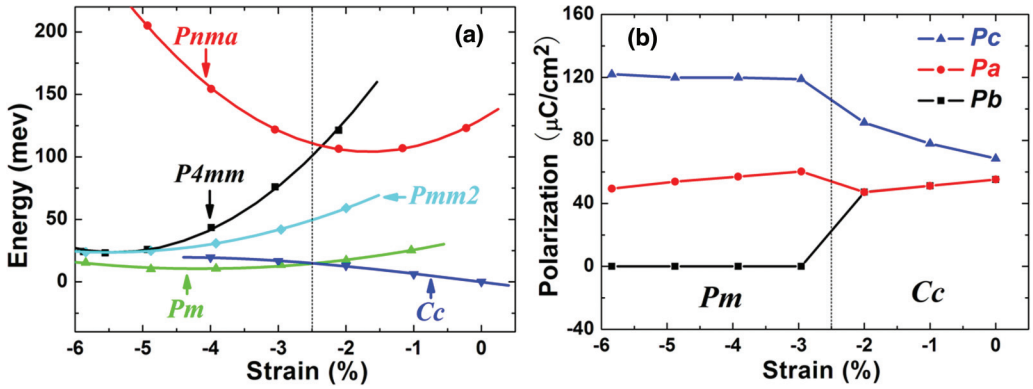

FIG. 5. (Color online) (a) Total energy as a function of misfit strain (%) of five different space groups—*Pmm*2, *Pm*, *P*4*mm*, *Pnma*, and *Cc* in (110) orientation. (b) Predicted polarization as a function of misfit strain. P_a, P_b, and P_c are along the a_m, b_m, and c_m directions, respectively.

approach ∼50 μC/cm^2, while the polarization along the b axis, P_b, diminishes at $\eta < -3\%$. This is consistent with the experimental polarization direction determined within the ac plane of the monoclinic lattice.

Although the monoclinic phase identified here shares the same space group Pm with the highly strained tetragonal-like BFO film in the (001) orientation, it has a unique crystal structure and promising physical behavior that is not available in the (001) orientation. Due to the large twin angle $\omega \sim 26^\circ$, the monoclinic c axis forms an angle ∼39° with the in-plane direction, which would result in a polarization projection of ∼90 μC/cm^2 based on the polarization value from our first-principles calculations. This in-plane polarization for the BFO film is much larger than the (001) orientated films.[29] The unique ferroelectric domain configuration here is different from previously observed 71° and 109° domains in (001) orientation, which may find interesting applications in domain wall nanoelectronics.[30] Moreover, as the film thickness increases, BFO film on LAO (110) substrate relaxes to a mixture of several phases with different lattice dimensions (to be published). This indicates a potential enhancement in piezoelectric property, as mixed BFO phases are highly sensitive to strain and external electrical field.[31] In addition, the strain-phase diagram for the BFO film in (110) orientation shows two ferroelectric phases with different structure distortion: Cc with $c/a \sim 1.0$ and Pm with $c/a \sim 1.2$, which indicates a feasible way to achieve larger magnetoelectric response as a result of structure softness.[32] The multiferroic behavior of this new BFO phase deserves further study.

IV. SUMMARY

In summary, the structure study by high resolution XRD shows that uniaxial strain instead of biaxial strain should be considered in studying the (110)-oriented epitaxial perovskite thin films. Uniaxial compressive strain of ∼4.5% from LAO (110) substrate greatly distorts the BFO crystal structure, which shows a giant c/a ratio of ∼1.24, a small monoclinic angle of ∼0.37°, and a large twin angle of ∼26°. A unique stripe ferroelectric domain structure is shown by modulation peaks in RSMs and PFM images. First-principles calculation predicts a strain-phase diagram for (110)-orientated BFO films, suggesting a potential routine to achieve novel functionalities in the BFO system. We hope this study will stimulate research interest in the physical behavior of BFO epitaxial films grown in the (110) orientation, instead of the extensively studied (001) orientation.

ACKNOWLEDGMENTS

The authors are grateful for technical support received at beamline BL14B1 of SSRF for the data collection under projects No. 11sr0395 and No. j10sr0092. P.Y. is supported by SSLS via NUS Core Support C-380-003-003-001. K.Y. acknowledges support from research project No. IMRE/10-1C0109 at the Institute of Materials Research and Engineering. K.P.O. acknowledges support from the Institute of High Performance Computing, A*STAR. J.W. acknowledges the grant support of A*Star, Singapore, conducted at National University of Singapore.

*Author to whom correspondence should be addressed: msewangj@nus.edu.sg

[1]P. Zubko, S. Gariglio, M. Gabay, P. Ghosez, and J. M. Triscone, Annu. Rev. Condens. Matter Phys. **2**, 141 (2011).

[2]D. G. Schlom, L. Q. Chen, C. B. Eom, K. M. Rabe, S. K. Streiffer, and J.-M. Triscone, Annu. Rev. Mater. Res. **37**, 589 (2007).

[3]J. P. Locquet, J. Perret, J. Fompeyrine, E. Machler, J. W. Seo, and G. Van Tendeloo, Nature (London) **394**, 453 (1998).

[4]I. Bozovic, G. Logvenov, I. Belca, B. Narimbetov, and I. Sveklo, Phys. Rev. Lett. **89**, 107001 (2002).

[5]K. J. Choi, M. Biegalski, Y. L. Li, A. Sharan, J. Schubert, R. Uecker, P. Reiche, Y. B. Chen, X. Q. Pan, V. Gopalan, L. Q. Chen, D. G. Schlom, and C. B. Eom, Science **306**, 1005 (2004).

[6]J. H. Lee, L. Fang, E. Vlahos, X. Ke, Y. W. Jung, L. F. Kourkoutis, J.-W. Kim, P. J. Ryan, T. Heeg, M. Roeckerath, V. Goian, M. Bernhagen, R. Uecker, P. C. Hammel, K. M. Rabe, S. Kamba, J. Schubert, J. W. Freeland, D. A. Muller, C. J. Fennie, P. Schiffer,

V. Gopalan, E. Johnston-Halperin, and D. G. Schlom, Nature (London) **466**, 954 (2010).

[7]M. Nakamura, Y. Ogimoto, H. Tamaru, M. Izumi, and K. Miyano, Appl. Phys. Lett. **86**, 182504 (2005).

[8]Y. Suzuki, H. Y. Hwang, S. W. Cheong, and R. B. van Dover, Appl. Phys. Lett. **71**, 140 (1997).

[9]H. Akoh, C. Camerlingo, and S. Takada, Appl. Phys. Lett. **56**, 1487 (1990).

[10]T. Zhao, A. Scholl, F. Zavaliche, K. Lee, M. Barry, A. Doran, M. P. Cruz, Y. H. Chu, C. Ederer, N. A. Spaldin, R. R. Das, D. M. Kim, S. H. Baek, C. B. Eom, and R. Ramesh, Nat. Mater. **5**, 823 (2006).

[11]C. Ederer and N. A. Spaldin, Phys. Rev. B **71**, 224103 (2005).

[12]A. J. Hatt, N. A. Spaldin, and C. Ederer, Phys. Rev. B **81**, 054109 (2010).

[13]H. Bea, B. Dupe, S. Fusil, R. Mattana, E. Jacquet, B. Warot-Fonrose, F. Wilhelm, A. Rogalev, S. Petit, V. Cros, A. Anane, F. Petroff, K. Bouzehouane, G. Geneste, B. Dkhil, S. Lisenkov, I. Ponomareva, L. Bellaiche, M. Bibes, and A. Barthelemy, Phys. Rev. Lett. **102**, 217603 (2009).

[14]R. J. Zeches, M. D. Rossell, J. X. Zhang, A. J. Hatt, Q. He, C. H. Yang, A. Kumar, C. H. Wang, A. Melville, C. Adamo, G. Sheng, Y. H. Chu, J. F. Ihlefeld, R. Erni, C. Ederer, V. Gopalan, L. Q. Chen, D. G. Schlom, N. A. Spaldin, L. W. Martin, and R. Ramesh, Science **326**, 977 (2009).

[15]G. Xu, J. Li, and D. Viehland, Appl. Phys. Lett. **89**, 222901 (2006).

[16]M. P. Cruz, Y. H. Chu, J. X. Zhang, P. L. Yang, F. Zavaliche, Q. He, P. Shafer, L. Q. Chen, and R. Ramesh, Phys. Rev. Lett. **99**, 217601 (2007).

[17]G. Kresse and J. Furthmüller, Phys. Rev. B **54**, 11169 (1996).

[18]J. P. Perdew, K. Burke, and M. Ernzerhof, Phys. Rev. Lett. **77**, 3865 (1996).

[19]P. E. Blöchl, O. Jepsen, and O. K. Andersen, Phys. Rev. B **49**, 16223 (1994).

[20]R. D. King-Smith and D. Vanderbilt, Phys. Rev. B **47**, 1651 (1993).

[21]D. Vanderbilt and R. D. King-Smith, Phys. Rev. B **48**, 4442 (1993).

[22]Y. Wakabayashi, D. Bizen, H. Nakao, Y. Murakami, M. Nakamura, Y. Ogimoto, K. Miyano, and H. Sawa, Phys. Rev. Lett. **96**, 017202 (2006).

[23]J. X. Zhang, Q. He, M. Trassin, W. Luo, D. Yi, M. D. Rossell, P. Yu, L. You, C. H. Wang, C. Y. Kuo, J. T. Heron, Z. Hu, R. J. Zeches, H. J. Lin, A. Tanaka, C. T. Chen, L. H. Tjeng, Y. H. Chu, and R. Ramesh, Phys. Rev. Lett. **107**, 147602 (2011).

[24]S. K. Streiffer, J. A. Eastman, D. D. Fong, C. Thompson, A. Munkholm, M. V. Ramana Murty, O. Auciello, G. R. Bai, and G. B. Stephenson, Phys. Rev. Lett. **89**, 067601 (2002).

[25]D. D. Fong, G. B. Stephenson, S. K. Streiffer, J. A. Eastman, O. Auciello, P. H. Fuoss, and C. Thompson, Science **304**, 1650 (2004).

[26]U. Gebhardt, N. V. Kasper, A. Vigliante, P. Wochner, H. Dosch, F. S. Razavi, and H. U. Habermeier, Phys. Rev. Lett. **98**, 096101 (2007).

[27]G. Catalan, A. Janssens, G. Rispens, S. Csiszar, O. Seeck, G. Rijnders, D. H. A. Blank, and B. Noheda, Phys. Rev. Lett. **96**, 127602 (2006).

[28]S. Prosandeev, I. A. Kornev, and L. Bellaiche, Phys. Rev. Lett. **107**, 117602 (2011).

[29]Z. Chen, X. Zou, W. Ren, L. You, C. Huang, Y. Yang, P. Yang, J. Wang, T. Sritharan, L. Bellaiche, and L. Chen, Phys. Rev. B **86**, 235125 (2012).

[30]G. Catalan, J. Seidel, R. Ramesh, and J. F. Scott, Rev. Mod. Phys. **84**, 119 (2012).

[31]J. X. Zhang, B. Xiang, Q. He, J. Seidel, R. J. Zeches, P. Yu, S. Y. Yang, C. H. Wang, Y. H. Chu, L. W. Martin, A. M. Minor, and R. Ramesh, Nat. Nanotechnol. **6**, 98 (2011).

[32]J. C. Wojdel and J. Iniguez, Phys. Rev. Lett. **105**, 037208 (2010).